ACS APPLIED MATERIALS & INTERFACES

Research Article

www.acsami.org

Arginine-Assisted Synthesis and Catalytic Properties of Single-Crystalline Palladium Tetrapods

Geng-Tao Fu,[†,§] Xian Jiang,[†,§] Rui Wu,[†] Shao-Hua Wei,[†] Dong-Mei Sun,[†] Ya-Wen Tang,*[,†] Tian-Hong Lu,[†] and Yu Chen*[,‡]

[†]Jiangsu Key Laboratory of New Power Batteries, Collaborative Innovation Center of Biomedical Functional Materials, School of Chemistry and Materials Science, Nanjing Normal University, Nanjing 210023, People's Republic of China

[‡]School of Materials Science and Engineering, Shaanxi Normal University, Xi'an 710062, People's Republic of China

Supporting Information

ABSTRACT: Noble metallic nanocrystals (NMNCs) with highly branched morphologies are an exciting new class of nanomaterials because of their great potential application in catalysis, sensing, optics, and electronics originating from their unique structures. Herein, we report a facile water-based method to synthesize high-quality palladium (Pd) tetrapods with the assistance of arginine molecule, which is more economical and environmentally friendly than the previous reported carbon monoxide (CO)-assisted synthesis in the organic system. During the synthesis, arginine molecule plays an essential role in controlling the tetrapod-like morphology. The as-synthesized Pd tetrapods have a potential application in the formic acid (HCOOH)-induced reduction of highly toxic hexavalent chromium (Cr(VI)) owing to their improved catalytic performance for the HCOOH decomposition.

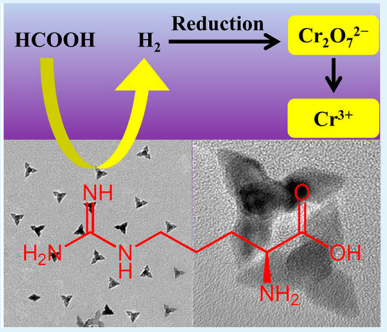

KEYWORDS: *arginine, palladium tetrapods, Cr(VI) reduction, formic acid, decomposition*

1. INTRODUCTION

Effectively controlled synthesis of noble metallic nanocrystals (NMNCs) with uniform and well-defined morphologies is a hot topic in catalysis due to the size-, surface structure-, and shape-dependent catalytic activity and durability.[1−13] Among various architectures of NMNCs, NMNCs with dendritic, multipod, star-like, and other anisotropic morphologies have attracted great interest due to their fascinating structural features, such as large surface areas, large number of multiple and high-angle edges, and sharp tips, which generally help to improve the catalytic activity and durability of NMNCs.[14−23]

As the highly chemically stable and widely applied catalytic material, Pd-NMNCs with branched and multipod shapes have been widely investigated.[14−19] For instance, Tilley and co-workers for the first time reported a facile hydrothermal approach for the synthesis of branch-like Pd-NMNCs containing less than 40% tripods in toluene solution.[19] Zheng and co-workers reported the carbon monoxide (CO)-assisted synthesis of single-crystalline Pd tetrapods in *N*,*N*-dimethylformamide (DMF) solution.[17] More recently, highly branched Pd tetrapods with pod length ca. 98 nm have also been successfully achieved through CO-assisted synthesis in sodium dodecyl sulfate solution.[18] However, most of these reports inevitably involve the contamination of organic solution or the use of very toxic gas. In keeping with the green chemistry principle, it is important to meet the environmentally friendly procedure for the synthesis of NMNCs.

Herein, we report a facile and environmentally friendly water-based route to directly synthesize tetrapod-like Pd-NMNCs (hereafter, Pd tetrapods) with the assistance of arginine molecule. Arginine (Scheme 1), an amino acid molecule, consists of four amine and one carboxyl groups, which provide more positive charge ($-NH_2^+$). To the best of our knowledge, there are no reports on the synthesis of Pd tetrapods in water-based amino acid system. Meanwhile, we for the first time use the {111} facets-enclosed Pd tetrapods to catalyze reduction of Cr(VI) to Cr(III) using formic acid (HCOOH) as hydrogen donor. The as-prepared Pd tetrapods exhibit enhanced catalytic activity compared to state-of-the-art commercial Pd black, originating from their improved catalytic performance for HCOOH decomposition.

Scheme 1. Structure of Arginine Molecule

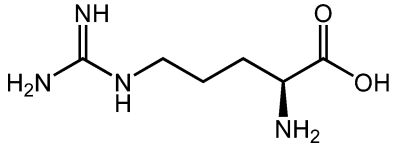

2. EXPERIMENTAL SECTION

2.1. Reagents and Chemicals. Arginine was purchased from Shanghai kayon Biological Technology Co., Ltd. (Shanghai, China). Polyvinylpyrrolidone (PVP, M_w = 30000), palladium chloride ($PdCl_2$),

Received: October 10, 2014
Accepted: December 3, 2014
Published: December 3, 2014

formaldehyde solution (HCHO, 40%), and formic acid (HCOOH) were purchased from Sinopharm Chemical Reagent Co., Ltd. (Shanghai, China). Commercial Pd black was purchased from Johnson Matthey Corporation. All reagents were of analytical reagent grade and used without further purification.

2.2. Preparation of Pd Tetrapods. In a typical synthesis, 0.5 mL of 0.05 M $PdCl_2$ solution, 4.0 mL of 0.05 M arginine, and 50 mg PVP were added into 4.0 mL deionized water. After the solution pH was adjusted to 12.0, 1.0 mL of HCHO solution (40%) was added into the mixture solution, and the solution was heated at 140 °C for 4 h. The obtained Pd tetrapods were collected by centrifugation and washed several times with ethanol solution.

2.3. Physical Characterizations. Transmission electron microscopy (TEM) and high-resolution TEM (HRTEM) were carried out on a JEOL JEM-2100F transmission electron microscopy operated at 200 kV. Energy dispersive X-ray (EDX) analysis was carried out on a JEOL JSM-7600F SEM. X-ray diffraction (XRD) patterns were obtained on a D/max-rC X-ray diffractometer with Cu Kα radiation (λ = 1.5406 Å) operated at 40 kV and 100 mA. X-ray photoelectron spectroscopy (XPS) measurements were performed on Thermo ESCALAB 250 with an Al anode. The ultraviolet and visible spectroscopy (UV−vis) data were recorded at room temperature on a Cary 50 spectrophotometer equipped with 1.0 cm quartz cells.

2.4. Catalytic Reduction of Cr(VI). Pd tetrapods were used for the catalytic reduction of Cr(VI) in aqueous solution. Prior to catalytic reaction, Pd tetrapods were irradiated with UV irradiation (185 and 254 nm) in air for 4 h to remove the capping agents (i.e., PVP and arginine).[24−27] Typically, 20 μL of Pd tetrapod aqueous solution (2.0 g L^{-1}) was added into 10 mL of mixture solution containing 4 mL of 2 mM $K_2Cr_2O_7$ solution and 0.2 mL of HCOOH (85%) at 50 °C under gentle magnetic stirring. At a regular time interval of 1 min, 0.5 mL of the mixture solution was withdrawn and diluted to 2 mL and then monitored by recording the time-dependent absorption spectra of the reduction reaction using a Cary 50 UV−vis spectrophotometer. For comparison, commercial Pd black was also used as heterogeneous catalyst for the catalytic reduction of Cr(VI).

2.5. Measurement of HCOOH Decomposition. For HCOOH decomposition, a total of 20 mg Pd tetrapods or commercial Pd black, 30 mL 0.5 M HCOOH solution were added into a three-necked flask at 50 °C under continuous stirring. The gases produced can be collected by draining saturated $NaHCO_3$ solution from a buret. Once CO_2 and H_2 gas are produced from the decomposition of HCOOH, the gas will go through the gas-guide tube and then into the $NaHCO_3$−replete sink and calibrated buret. Because the $NaHCO_3$ solution does not absorb CO_2 and H_2, the generated gases come into the calibrated buret, and the $NaHCO_3$ solution in the buret is drained by the gas. Thus, the volume of the gas produced from the decomposition of HCOOH over the catalyst can be recorded through the change of the solution volume.

2.6. Electrochemical Instrument. The electrochemical experiments were performed on CHI 660 C electrochemical analyzer at 30 ± 1 °C. A standard three-electrode system was used, which consisted of glassy carbon working electrode, a saturated calomel reference electrode (SCE), and a platinum wire as the auxiliary electrode.

3. RESULTS AND DISCUSSION

3.1. Physicochemical Characterization of Pd Tetrapods. The morphology of the as-prepared Pd nanocrystals was first investigated by TEM. As observed, nearly all of the two-dimensional (2D) projections of Pd nanocrystals under TEM look like the three-branched nanostructures (Figure 1A,B and Figure S1, Supporting Information). Additionally, most of Pd nanocrystals exhibit a darker contrast in the center relative to the branches (Figure 1B), implying planar tripod-like nanostructures are actually the tetrapods. The tetrapod morphology of Pd nanocrystals is further supported by the tilting TEM studies (Figure 1C). After the sample is tilted, the fourth branch is revealed obviously. From the magnified TEM

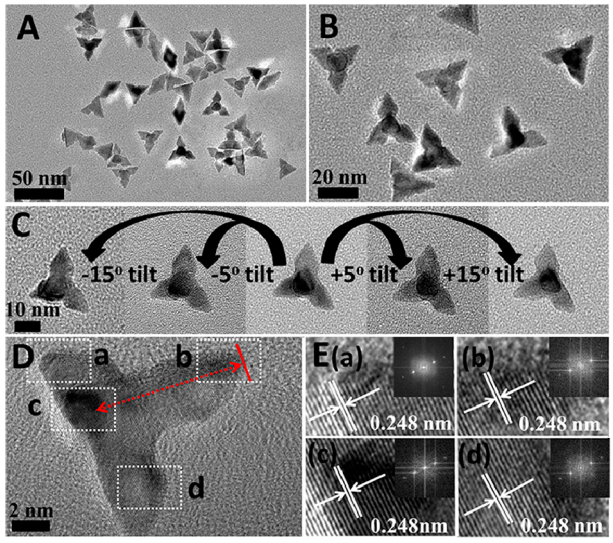

Figure 1. (A) Typical and (B) magnified TEM images of Pd tetrapods. (C) TEM images of an individual Pd tetrapod tilted at different angles. (D) HRTEM image of an individual Pd tetrapod. (E) Magnified HRTEM images obtained from regions a, b, c, and d marked by squares in panel D. The top-right insets in panel E show the corresponding FFT patterns.

image of an individual Pd tetrapod (Figure 1D), the average apex-to-center dimension (i.e., each pot size) of Pd tetrapods is estimated to be 10 ± 2 nm in length. More structural information was provided by HRTEM. The lattice spacing of fringes on each pod branches is ca. 0.248 nm (Figure 1E), close to the face-centered cubic (fcc) Pd {111} facets (0.246 nm, JCPDS card no. 46-1043), demonstrating that Pd tetrapods are grown along the {111} direction. The fast Fourier transform (FFT) patterns indicate the single crystalline nature of the branches (Figure 1E, insets). Such highly crystalline Pd tetrapods are expected be a good catalyst due to their unique branched structure, which effectively provides big active surface area and restrains the aggregation of nanocrystals in the course of catalytic reaction. EDX and XRD patterns were applied to investigate the chemical composition and crystalline structure of the products. EDX measurement demonstrates that the products mainly contain metal Pd (Figure S2, Supporting Information). XRD diffraction peaks at 40.1, 46.6, 67.9, and 82.0° can be easily assigned to the {111}, {200}, {220}, and {311} crystal facets of fcc Pd (JCPDS card no. 46-1043), showing a high degree of metallic character and crystallinity (Figure 2A). Based on the Scherrer equation, the average particle size of Pd tetrapods is calculated to be ca. 10.7 nm. XPS measurement shows that the binding energy of Pd $3d_{5/2}$ and Pd

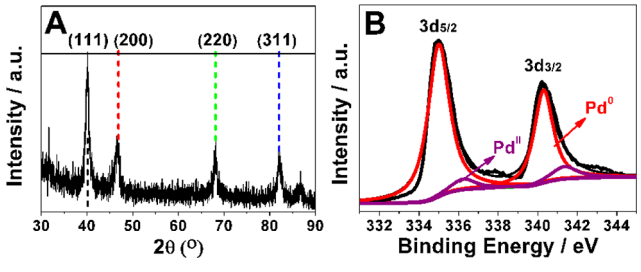

Figure 2. (A) XRD pattern and (B) Pd 3d XPS spectrum of Pd tetrapods.

dx.doi.org/10.1021/am506965f | ACS Appl. Mater. Interfaces 2014, 6, 22790−22795

$3d_{3/2}$ locate at 335.0 and 340.25 eV (Figure 2B), which are almost coincident with the standard values of bulk Pd (334.90 and 340.15 eV). Meanwhile, the percentage of Pd^0 in Pd tetrapods is ca. 92.3%, indicating that Pd^{II} species is successfully reduced to form metallic Pd.

3.2. Formation Mechanism of Pd Tetrapods. To clearly understand the formation mechanism of Pd tetrapods, the controlled experiments were conducted. It is found that the use of arginine is critical for the formation of Pd tetrapods. In the absence of arginine, only irregular, small nanoparticles are obtained (Figure 3A), indicating that arginine mainly acts as a

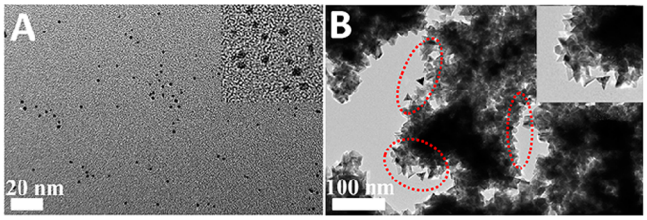

Figure 3. TEM images of Pd nanoparticles prepared under the same conditions as in Figure 1 with the exception of the absence of (A) arginine and (B) PVP molecules.

morphology controlling agent. Meanwhile, we also observe that PVP is important but not essential for the generation of Pd tetrapods. In the absence of PVP, the final products are dominated by the random-aggregation Pd nanoparticles (Figure 3B). However, the careful observation shows that a small amount of regular nanocrystals such as tetrapods and tetrahedra also exist (see cycle), indicating that PVP mainly served as a protecting and a dispersing agent. These results suggest that the formation of Pd tetrapods can be attributed to the existence of arginine molecules. Recently, small molecule adsorbates (e.g., CO, formate ions, and amino) assisted synthesis has emerged as a power strategy to control the surface structure of Pd nanocrystals.[9−11,17,18] For example, the coadsorption of sodium dodecyl sulfate and CO on Pd{111} was crucial to the formation of the hierarchical tetrapod Pd nanocrystals.[18] Similarly, the adsorption of the formate ions on Pd surface could control the dynamical imbalance of the growth and dissolution rate, which facilitated the growth of specific Pd nanocrystals.[10] Thus, we presumed that the {111}-enclosed Pd tetrapods mainly originated from the preferential and strong chemisorption of amino acid on Pd {111} facets. In order to confirm such conclusion, we introduce the same molar amount of L-lysine to substitute arginine in our synthetic system. As expected, the tetrapod-like Pd nanocrystals can also be obtained (Figure S3, Supporting Information).

When arginine is introduced into the $PdCl_2$ solution, the more stable arginine-Pd^{II} complex became the dominant species, which is favorable for the morphological control due to the slower reduction kinetics. The Pd^{II} species can easily coordinate with arginine molecule, which is confirmed by UV−vis measurement (Figure 4). Upon addition of arginine solution (pH 2.0) to $PdCl_2$ solution (pH 2.0), the characteristic absorption peaks of $PdCl_2$ at 238 and 316 nm completely vanish (Figure 4A). In addition, as the pH value of the arginine-Pd^{II} complex is adjusted to 12.0, the characteristic absorption peaks at 210 occur red shift (Figure 4B), accompanying a color change of brown to colorless (Figure 4B, inset). In contrast, a lot of red $PdO{\cdot}H_2O$ precipitates generate immediately after the pH value of the $PdCl_2$ solution is adjusted to 12.0 (Figure S4,

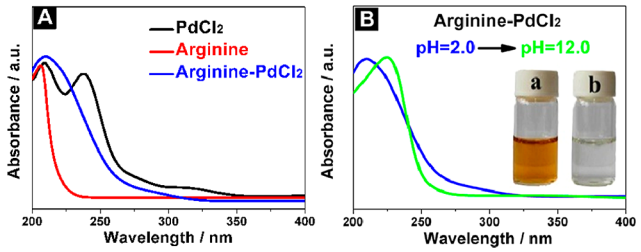

Figure 4. (A) UV−vis spectra of arginine solution (pH 2.0, red line), $PdCl_2$ solution (pH 2.0, black line) and the mixture solution of arginine and $PdCl_2$ (pH 2.0, blue line). (B) the mixture solution of arginine and $PdCl_2$ at pH values of 2.0 (blue line) and 12.0 (green line); (inset) photographs of the mixture solution of arginine and $PdCl_2$ at (a) pH 2.0 and (b) 12.0.

Supporting Information). Thus, these results confirm $PdCl_2$ can interact with arginine to generate stable arginine-Pd^{II} complex, and the solution pH determines the coordination forms of arginine-Pd^{II} complex. Further electrochemical measurements show the reduction potential of arginine-Pd^{II} complex negatively shifts with the increase of pH (Figure S5, Supporting Information). Compared with the synthesis of Pd tetrapods (pH 12.0), when the value of pH is decreased to pH 7.0, flat tetrahedral or trigonal bipyramidal Pd nanocrystals are obtained (Figure S6, Supporting Information). These facts indicate the slower reduction rate of arginine-Pd^{II} complex is necessary for the formation of Pd tetrapods.

3.3. Catalytic Tests. Hexavalent chromium (Cr(VI)), one of the most common pollutants, is proven to have high toxicity, mutagenicity, and carcinogenicity, which increases the risk of lung cancer via chronic inhalation.[28−32] However, trivalent chromium (Cr(III)) is nontoxic and, in trace amounts, is an essential nutrient for humans. Thus, it is highly desirable to develop an efficient and eco-friendly catalytic system to transform Cr(VI) to Cr(III). Herein, the reduction of Cr(VI) to Cr(III) by HCOOH is chosen as a model reaction to study the catalytic performance of Pd tetrapods. Potassium dichromate ($K_2Cr_2O_7$) is chosen as one of the representative Cr(VI) compounds. It is well-known that the characteristic absorption peak of Cr(VI) is centered at 350 nm, originating from the ligand (oxygen) to metal (Cr(VI) charge transfer transition.[32,33] Thus, the reduction reaction processes can be monitored by UV−vis. In the absence of catalyst, the absorption intensity at 350 nm remains almost unchanged over 30 min, suggesting the reduction cannot proceed without catalyst (Figure 5A). When a certain amount of Pd tetrapods are introduced, the absorption peak at 350 nm gradually decreases and vanishes within 5 min (Figure 5B), accompanying a color change of yellow to colorless (Figure 5B, inset), indicating the successfully reduction of Cr(VI). The formation of Cr(III) is confirmed by adding an excess of NaOH solution, where the color of solution changes from colorless to green, indicating the formation of hexahydroxochromate (III) (Figure S7, Supporting Information).[32−35] It is worth noting that the reduction time of Cr(VI) on commercial Pd black (20 min, Figure 5C) is much longer than that on Pd tetrapods, indicating Pd tetrapods possesses excellent catalytic activity for Cr(VI) reduction. Additionally, the reaction rate constant κ is calculated from the slope of the linear section of the plots of $\ln(C_t/C_0)$ versus reaction time (t) (Figure 5D). Compared with Pd black catalyst (κ = 0.156 min^{-1}), the Pd tetrapods

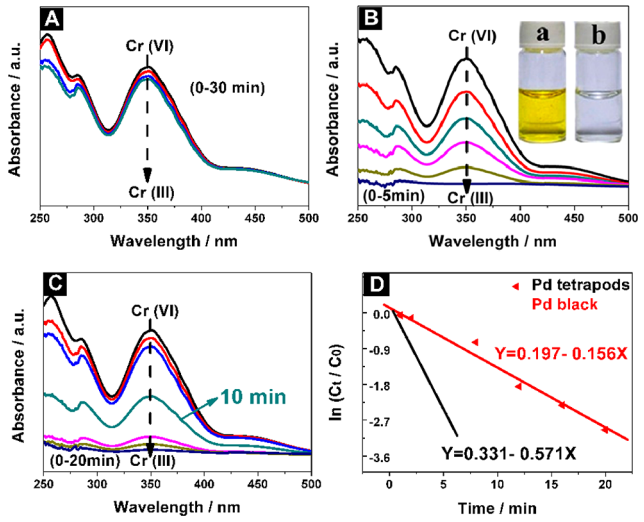

Figure 5. UV−vis spectra for successive reduction of $Cr_2O_7^{2-}$ with HCOOH at 50 °C: (A) catalyst-free, (B) catalyzed by the Pd tetrapods, (C) catalyzed by the commercial Pd black. (B, inset) photographs of (a) Cr(VI) and (b) Cr(III) ion solutions. (D) The relationship between $\ln(C_t/C_0)$ and reaction time (t).

exhibit a better catalytic activity for the reduction of Cr(VI) to Cr(III) (κ = 0.571 min^{-1}).

Generally, it is widely accepted that the chemical decomposition of HCOOH via a dual-path mechanism including of indirect and direct pathways, that is, the dehydration pathway (HCOOH → CO + H_2O) and dehydrogenation pathway (HCOOH → CO_2 + H_2).[33,35−38] Recent theoretical calculations on HCOOH decomposition on Pd{111} unanimously demonstrated that the dehydrogenation involved a much lower barrier than the dehydration pathway.[36−38] Thus, CO_2 and H_2 were proposed as the highly preferred products for HCOOH decomposition on {111}-facet enclosed Pd catalysts. According to the above discussion, the mechanism of HCOOH decomposition is illustrated schematically in Scheme 2. Specifically, HCOOH (i,e., hydrogen donor)

Scheme 2. Schematic Representation of Cr(VI) Reduction on Pd Catalyst

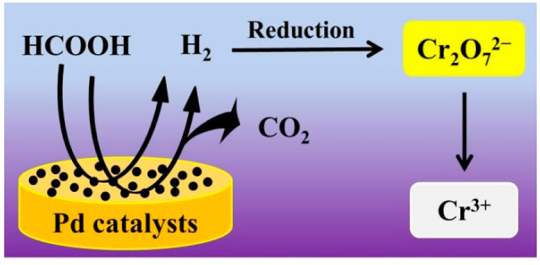

adsorbs on the surface of Pd catalyst, resulting in the degradation of HCOOH into CO_2 and H_2, and consequently reducing Cr(VI) to Cr(III) through H_2 transfer ($Cr_2O_7^{2-}$ + $8H^+$ + $3H_2$ → $2Cr^{3+}$ + $7H_2O$).

Catalytic performance of Pd tetrapods and Pd black for the chemical decomposition of HCOOH were investigated. Figure 6A displays the plots of the time versus gas volume produced from the catalytic decomposition of HCOOH using Pd tetrapods and Pd black as catalysts. The gas volume produced from the decomposition of HCOOH on Pd tetrapods and Pd

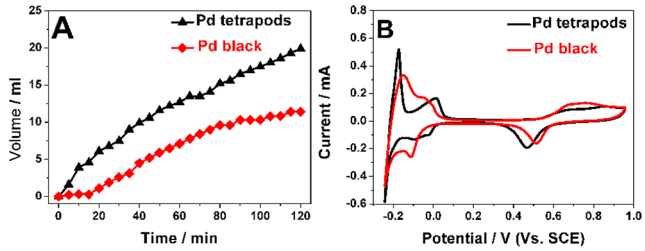

Figure 6. (A) Plots of time versus gas volume produced from the catalytic decomposition of HCOOH over Pd tetrapods and Pd black in 0.5 M HCOOH solution. (B) Cyclic voltammograms of Pd tetrapods and Pd black in N_2-saturated 0.5 M H_2SO_4 solution, sweep rate 50 mV s^{-1}.

black within 2 h is 20.0 and 11.0 mL, respectively. This fact demonstrates the chemical decomposition of HCOOH on Pd tetrapods surface is easier than that on Pd black, attributing to the abundant exposed {111} facets with high activity on Pd tetrapods.[36,38−40] On the other hand, electrochemical measurements indicate the active surface area (11.4 m^2 g^{-1}) of Pd tetrapods is 1.65 times bigger than that (6.9 m^2 g^{-1}) of Pd black (Figure 6B), which also contributes to the enhanced catalytic performance for the reduction of Cr(VI) due to area effect.

4. CONCLUSIONS

In summary, this work shows an easy, one-pot, and environmentally friendly procedure for the synthesis of Pd tetrapods. The presence of arginine is key in controlling the shape/surface structure of the Pd nanocrystals due to the preferential chemisorption of arginine on Pd {111} facets and the change in reduction kinetics of Pd^{II} precursor. Owing to the faster decomposition of HCOOH on Pd tetrapods and bigger active surface area of Pd tetrapods, the as-prepared Pd tetrapods exhibit substantially enhanced catalytic performance for the reduction of highly toxic aqueous Cr(VI) relative to the commercial Pd black.

■ ASSOCIATED CONTENT

Ⓢ Supporting Information

Experimental and characterization details. This material is available free of charge via the Internet at http://pubs.acs.org.

■ AUTHOR INFORMATION

Corresponding Authors

*E-mail: tangyawen@njnu.edu.cn.

*E-mail: ndchenyu@gmail.com.

Author Contributions

§Dr. G. T. Fu and X. Jiang contributed equally to this work.

Notes

The authors declare no competing financial interest.

■ ACKNOWLEDGMENTS

This work is supported by the National Natural Science Foundation of China (21473111, 21376122, and 21273116), the United Fund of NSFC and Yunnan Province (U1137602), the Natural Science Foundation of Jiangsu Province (BK20131395), the Fundamental Research Funds for the Central Universities (GK201402016), and a project funded by the Priority Academic Program Development of Jiangsu Higher Education Institutions.

REFERENCES

(1) Yang, S.; Luo, X. Mesoporous Nano/Micro Noble Metal Particles: Synthesis and Applications. *Nanoscale* **2014**, *6*, 4438−4457.
(2) Zhang, H.; Jin, M.; Xia, Y. Noble-Metal Nanocrystals with Concave Surfaces: Synthesis and Applications. *Angew. Chem., Int. Ed.* **2012**, *51*, 7656−7673.
(3) Quan, Z.; Wang, Y.; Fang, J. High-Index Faceted Noble Metal Nanocrystals. *Acc. Chem. Res.* **2012**, *46*, 191−202.
(4) Cheong, S.; Watt, J. D.; Tilley, R. D. Shape Control of Platinum and Palladium Nanoparticles for Catalysis. *Nanoscale* **2010**, *2*, 2045−2053.
(5) Xiong, Y.; Xia, Y. Shape-Controlled Synthesis of Metal Nanostructures: The Case of Palladium. *Adv. Mater.* **2007**, *19*, 3385−3391.
(6) Chen, J.; Lim, B.; Lee, E. P.; Xia, Y. Shape-Controlled Synthesis of Platinum Nanocrystals for Catalytic and Electrocatalytic Applications. *Nano Today* **2009**, *4*, 81−95.
(7) Gong, M.; Fu, G.; Chen, Y.; Tang, Y.; Lu, T. Autocatalysis and Selective Oxidative Etching Induced Synthesis of Platinum−Copper Bimetallic Alloy Nanodendrites Electrocatalysts. *ACS Appl. Mater. Interfaces* **2014**, *6*, 7301−7308.
(8) Cunci, L.; Velez, C. A.; Perez, I.; Suleiman, A.; Larios, E.; José-Yacamán, M.; Watkins, J. J.; Cabrera, C. R. Platinum Electrodeposition at Unsupported Electrochemically Reduced Nanographene Oxide for Enhanced Ammonia Oxidation. *ACS Appl. Mater. Interfaces* **2014**, *6*, 2137−2145.
(9) Nguyen, T.-T.; Pan, C.-J.; Liu, J.-Y.; Chou, H.-L.; Rick, J.; Su, W.-N.; Hwang, B.-J. Functional Palladium Tetrapod Core of Heterogeneous Palladium−Platinum Nanodendrites for Enhanced Oxygen Reduction Reaction. *J. Power Sources* **2014**, *251*, 393−401.
(10) Wang, Q.; Wang, Y.; Guo, P.; Li, Q.; Ding, R.; Wang, B.; Li, H.; Liu, J.; Zhao, X. S. Formic Acid-Assisted Synthesis of Palladium Nanocrystals and Their Electrocatalytic Properties. *Langmuir* **2014**, *30*, 440−446.
(11) Chen, M.; Wu, B. H.; Yang, J.; Zheng, N. F. Small Adsorbate-Assisted Shape Control of Pd and Pt Nanocrystals. *Adv. Mater.* **2012**, *24*, 862−879.
(12) Hu, B.; Ding, K.; Wu, T.; Zhou, X.; Fan, H.; Jiang, T.; Wang, Q.; Han, B. Shape Controlled Synthesis of Palladium Nanocrystals by Combination of Oleylamine and Alkylammonium Alkylcarbamate and Their Catalytic Activity. *Chem. Commun.* **2010**, *46*, 8552−8554.
(13) Wang, Y.; Xie, S.; Liu, J.; Park, J.; Huang, C. Z.; Xia, Y. Shape-Controlled Synthesis of Palladium Nanocrystals: A Mechanistic Understanding of the Evolution from Octahedrons to Tetrahedrons. *Nano Lett.* **2013**, *13*, 2276−2281.
(14) Zhao, R.; Fu, G.; Zhou, T.; Chen, Y.; Zhu, X.; Tang, Y.; Lu, T. Multi-Generation Overgrowth Induced Synthesis of Three-Dimensional Highly Branched Palladium Tetrapods and Their Electrocatalytic Activity for Formic Acid Oxidation. *Nanoscale* **2014**, *6*, 2776−2781.
(15) Chu, Y.-T.; Chanda, K.; Lin, P.-H.; Huang, M. H. Aqueous Phase Synthesis of Palladium Tripod Nanostructures for Sonogashira Coupling Reactions. *Langmuir* **2012**, *28*, 11258−11264.
(16) Zhu, H.; Li, G.; Chi, Q.; Zhao, Y.; Liu, H.; Li, J.; Huang, T. Controlled Synthesis of Tetrapod/Mitsubishi-Like Palladium Nanocrystals. *CrystEngComm* **2012**, *14*, 1531−1533.
(17) Dai, Y.; Mu, X.; Tan, Y.; Lin, K.; Yang, Z.; Zheng, N.; Fu, G. Carbon Monoxide-Assisted Synthesis of Single-Crystalline Pd Tetrapod Nanocrystals through Hydride Formation. *J. Am. Chem. Soc.* **2012**, *134*, 7073−7080.
(18) Zhu, H.; Li, G.; Lv, X.; Zhao, Y.; Huang, T.; Liu, H.; Li, J. Controlled Synthesis of Hierarchical Tetrapod Pd Nanocrystals and Their Enhanced Electrocatalytic Properties. *RSC Adv.* **2014**, *4*, 6535−6539.
(19) Watt, J.; Young, N.; Haigh, S.; Kirkland, A.; Tilley, R. D. Synthesis and Structural Characterization of Branched Palladium Nanostructures. *Adv. Mater.* **2009**, *21*, 2288−2293.
(20) Ma, L.; Wang, C.; Gong, M.; Liao, L.; Long, R.; Wang, J.; Wu, D.; Zhong, W.; Kim, M. J.; Chen, Y.; Xie, Y.; Xiong, Y. Control Over the Branched Structures of Platinum Nanocrystals for Electrocatalytic Applications. *ACS Nano* **2012**, *6*, 9797−9806.
(21) Liu, Z.; Fu, G.; tang, y.; Sun, D.; Chen, Y.; Lu, T. A Facile, One-Pot Synthesis of Highly Branched Au Nanocorals and Their Enhanced Electrocatalytic Activity for Ethanol Oxidation. *CrystEngComm* **2014**, *16*, 8576−8581.
(22) Fu, G.; Jiang, X.; Gong, M.; Chen, Y.; Tang, Y.; Lin, J.; Lu, T. Highly Branched Platinum Nanolance Assemblies by Polyallylamine Functionalization as Superior Active, Stable, and Alcohol-Tolerant Oxygen Reduction Electrocatalysts. *Nanoscale* **2014**, *6*, 8226−8234.
(23) Zhu, M.; Lei, B.; Ren, F.; Chen, P.; Shen, Y.; Guan, B.; Du, Y.; Li, T.; Liu, M. Branched Au Nanostructures Enriched with a Uniform Facet: Facile Synthesis and Catalytic Performances. *Sci. Rep.* **2014**, *4*, 5259−5266.
(24) Crespo-Quesada, M.; Andanson, J. M.; Yarulin, A.; Lim, B.; Xia, Y.; Kiwi-Minsker, L. UV−Ozone Cleaning of Supported Poly (vinylpyrrolidone)-Stabilized Palladium Nanocubes: Effect of Stabilizer Removal on Morphology and Catalytic Behavior. *Langmuir* **2011**, *27*, 7909−7916.
(25) Fu, G.; Liu, C.; Wu, R.; Chen, Y.; Zhu, X.; Sun, D.; Tang, Y.; Lu, T. L-Lysine Mediated Synthesis of Platinum Nanocuboids and Their Electrocatalytic Activity towards Ammonia Oxidation. *J. Mater. Chem. A* **2014**, *2*, 17883−17888.
(26) Fu, G.; Jiang, X.; Tao, L.; Chen, Y.; Lin, J.; Zhou, Y.; Tang, Y.; Lu, T. Polyallylamine Functionalized Palladium Icosahedra: One-Pot Water-Based Synthesis and Their Superior Electrocatalytic Activity and Ethanol Tolerant Ability in Alkaline Media. *Langmuir* **2013**, *29*, 4413−4420.
(27) Fu, G.; Wu, K.; Lin, J.; Tang, Y.; Chen, Y.; Zhou, Y.; Lu, T. One-Pot Water-Based Synthesis of Pt−Pd Alloy Nanoflowers and Their Superior Electrocatalytic Activity for the Oxygen Reduction Reaction and Remarkable Methanol-Tolerant Ability in Acid Media. *J. Phys. Chem. C* **2013**, *117*, 9826−9834.
(28) Stearns, D. M.; Kennedy, L. J.; Courtney, K. D.; Giangrande, P. H.; Phieffer, L. S.; Wetterhahn, K. E. Reduction of Chromium (VI) by Ascorbate Leads to Chromium−DNA Binding and DNA Strand Breaks in Vitro. *Biochem.* **1995**, *34*, 910−919.
(29) Elliott, D. W.; Zhang, W.-X. Field Assessment of Nanoscale Bimetallic Particles for Groundwater Treatment. *Environm. Sci. Technol.* **2001**, *35*, 4922−4926.
(30) Borah, B. J.; Saikia, H.; Bharali, P. Reductive Conversion of Cr (VI) to Cr (III) over Bimetallic CuNi Nanocrystals At Room Temperature. *New J. Chem.* **2014**, *38*, 2748−2751.
(31) Bhowmik, K.; Mukherjee, A.; Mishra, M. K.; De, G. Stable Ni Nanoparticle−Reduced Graphene Oxide Composites for the Reduction of Highly Toxic Aqueous Cr (VI) at Room Temperature. *Langmuir* **2014**, *30*, 3209−3216.
(32) Huang, Y.; Ma, H.; Wang, S.; Shen, M.; Guo, R.; Cao, X.; Zhu, M.; Shi, X. Efficient Catalytic Reduction of Hexavalent Chromium Using Palladium Nanoparticle-Immobilized Electrospun Polymer Nanofibers. *ACS Appl. Mater. Interfaces* **2012**, *4*, 3054−3061.
(33) Dandapat, A.; Jana, D.; De, G. Pd Nanoparticles Supported Mesoporous γ-Al_2O_3 Film as A Reusable Catalyst for Reduction of Toxic Cr^{VI} to Cr^{III} in Aqueous Solution. *Appl. Catal., A* **2011**, *396*, 34−39.
(34) Abass, E.; Alireza, M.; Reza, V. Chromium (III) Removal and Recovery from Tannery Wastewater by Precipitation. *Am. J. Appl. Sci.* **2005**, *2*, 1471−1473.
(35) Omole, M. A.; K'Owino, I. O.; Sadik, O. A. Palladium Nanoparticles for Catalytic Reduction of Cr (VI) Using Formic Acid. *Appl. Catal., B* **2007**, *76*, 158−167.
(36) Zhang, R.; Liu, H.; Wang, B.; Ling, L. Insights into the Preference of CO_2 Formation from HCOOH Decomposition on Pd Surface: A Theoretical Study. *J. Phys.Chem. C* **2012**, *116*, 22266−22280.
(37) Mori, K.; Dojo, M.; Yamashita, H. Pd and Pd−Ag Nanoparticles within a Macroreticular Basic Resin: An Efficient Catalyst for Hydrogen Production from Formic Acid Decomposition. *ACS Catal.* **2013**, *3*, 1114−1119.

(38) Hu, C.; Ting, S.-W.; Chan, K.-Y.; Huang, W. Reaction Pathways Derived from DFT for Understanding Catalytic Decomposition of Formic Acid into Hydrogen on Noble Metals. *Int. J. Hydrogen Energy* **2012**, *37*, 15956−15965.
(39) Zhou, S.; Qian, C.; Chen, X. Comparative Theoretical Study of Adsorption and Dehydrogenation of Formic Acid, Hydrazine and Isopropanol on Pd (111) Surface. *Catal. Lett.* **2011**, *141*, 726−734.
(40) Luo, Q.; Feng, G.; Beller, M.; Jiao, H. Formic Acid Dehydrogenation on Ni (111) and Comparison with Pd (111) and Pt (111). *J. Phys. Chem. C* **2012**, *116*, 4149−4156.